

Biological impedance cross evaluation and imaging from composite measurements of magnetic and electrical methods

Peng Ran^a, Xiaoming Xiao^{b,*}, Wei He^b and Zhangyong Li^a

^a*Chongqing Municipal Level Key Laboratory of Photoelectronic Information Sensing and Transmitting Technology, Chongqing University of Posts and Telecommunications, 400065, Chongqing 400065, China*

^b*State Key Laboratory of Power Transmission Equipment & System Security and New Technology, 400044, Chongqing, China*

Abstract. Because of the need for rapid detection and location of diseases in clinical applications, this work proposes a composite measurement of magnetic induction tomography (MIT) and electrical impedance tomography (EIT). This paper is composed of the following aspects: portable and integral hardware design, stable dual constant-current sources, the composite detection method, cross-plane data acquisition, 3-dimensional image reconstruction and so on. A qualitative evaluation of conductivity, resolution and relative position error were taken by combining the EIT and MIT methods via the experiment model. The sensitivities of both methods were analyzed to improve the imaging results. The reconstruction results reveal that the system is capable of obtaining better physiological measurements, which is very useful in clinical monitoring, quick medical diagnosing and preliminary screening of community health.

Keywords: Bioelectrical impedance measurement, magnetic induction tomography, cross evaluation and imaging, 3-dimensional image

1. Introduction

Although traditional detection technology such as X-rays, CT scans, Magnetic Resonance Imaging (MRI), Positron Emission Tomography (PET) and ultrasounds can accurately determine the critical nature, range and degree of a disease, they are incapable of continuous imaging for monitoring and rapid detection. Electrical impedance tomography (EIT) [1] and magnetic induction tomography (MIT) [2] are based on the physical principle that different human tissue figures have different conductivities. We could measurement the useful information of the body to extract the conductive properties of internal information and reconstruct the image distribution of electrical parameters inside the body or its change, providing useful information for medical diagnosis [3-6].

* Address for correspondence: Xiaoming Xiao, State Key Laboratory of Power Transmission Equipment & System Security and New Technology, 400044, Chongqing, China. Tel.: +86 18875035568; Fax: 023-62471404; E-mail: xiaoxiaoming@cqu.edu.cn.

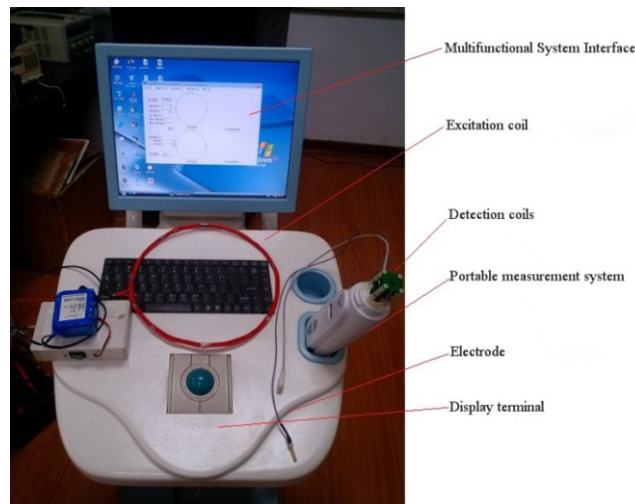


Fig. 1. Composing of the imaging system.

MIT is a noninvasive and contactless medical functional imaging technique that is not affected by the shield effect of the human skull. However, MIT has difficulty obtaining useful signals deep in the brain, and the number of measuring is restricted by the relatively large coil. EIT is often used in models of fixed size and fixed electrode locations, which are usually applied in a certain part of the human body. Nevertheless, the fixed electrodes do not fit individual structural differences [7].

Combining MIT with EIT introduces a system that takes multi-frequency and dual-detection terminals with a flexible imaging strategy at any time. By this means, we can conduct cross validation based on multi characters, including the change electrical characteristics of human tissue (such as cancer, brain glioma preliminary detection, etc.) and the dynamic monitoring of physiological activities (such as breathing and heart beat).

2. Method and realization

2.1. System features

The imaging system is flexible and well combined. As shown in Figure 1, the sensor coils of MIT are fixed as the front probe, and the excitation and detection electrodes of EIT are led out through wires. When taking measurements, the magnetic signals are picked first to judge the position and state of the illness, and then electrical signals are picked to get encryption measurement and imaging. This well supports the follow-up algorithm and image reconstruction and overcomes the model error produced by individual differences and the different medical treatments [8, 9].

2.2. Measurement example analysis

For the hemisphere detection model, the model of 8-16 sensors pick up the MIT signals in Figure 2(a). As the sensors' coils are relatively large compared to the imaging area, accuracy is insufficient

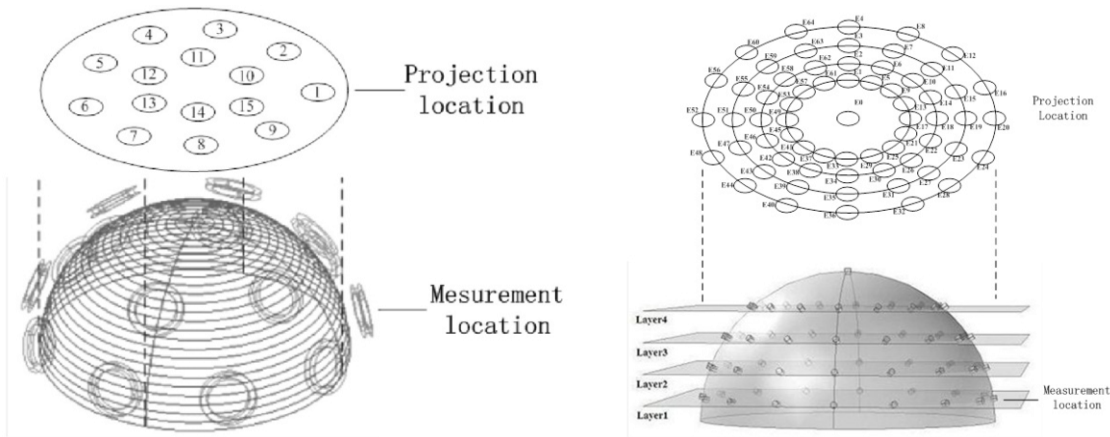


Fig. 2. (a) MIT Projection Diagram and (b) EIT Measurement Position Diagram.

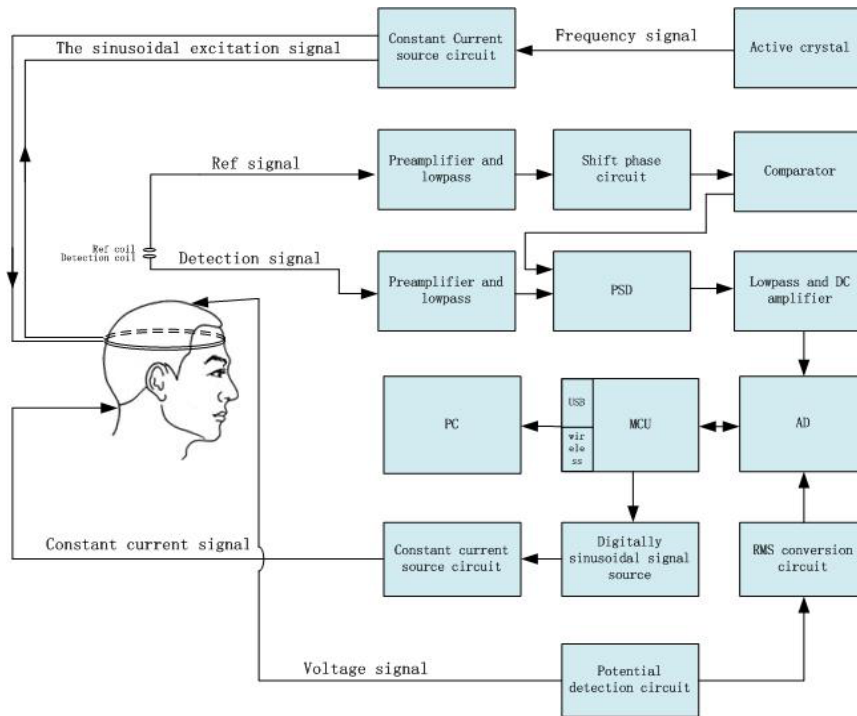


Fig. 3. System configuration diagram.

for three-dimensional imaging. In order to increase sampling density, the EIT is introduced, as in Figure 2(b).

The measurement points are distributed in four different layers, and each layer has sixteen electrodes, which are spaced equidistantly and annularly on the edge of the horizontal hemisphere. At the vertical hemisphere, these electrodes are distributed on eight group tangent planes, which cross the vertex of the hemisphere and intersect with the mentioned four different horizontal layers at right angles. By such division, each tangent plane includes nine electrodes; the angle between the electrodes is unequal, but they are axially symmetrical, which greatly increases the combination of independent

measurement data and makes space imaging possible [10].

2.3. System implementation

In order to realize the detection needs of the two measurement methods, the system designed an independent excitation source to generate the alternating primary magnetic field, as shown in Figure 3. The sinusoidal current injected in the excitation coil is 20 mA at 10 MHz [11]. The source of the sinusoidal signal is the highly stable and temperature-compensated crystal oscillator.

The MIT method uses phase-sensitive detection. To minimize the influence of the primary magnetic field signal, an axial gradiometer is used as the sensor in our system. The axial gradiometer consists of two detection coils and one shield coil. The shield coil is very important in rejecting capacitive coupling, and the two detection coils are located on both sides of the shield coil. The outside detection coil is the recalled signal coil, and the other detection coil is the recalled reference coil.

3. Simulation analysis of the composite measurement

The EIT numerical simulation study was carried out using COMSOL Multiphysics 4.1 for 3-D model establishment and forward problem simulation. Voltage analysis, parameters evaluation and image reconstruction took place in Matlab (Ver: 7.11.0).

3.1. Simulation model construction

As shown in Figure 4(a), this paper constructs a hemisphere with a radius of 10 cm. The conductivity of the liquid in the hemisphere is 0.2 Sm^{-1} . The other sphere has a hemisphere radius of 2 cm, and the conductivity of the sphere is 0.2 Sm^{-1} . The sphere was placed in b_0 ($x=0 \text{ cm}$, $y=2.5 \text{ cm}$), b_1 ($x=0 \text{ cm}$, $y=5 \text{ cm}$), b_2 ($x=0 \text{ cm}$, $y=7.5 \text{ cm}$), c_0 ($x=2.5 \text{ cm}$, $y=2.5 \text{ cm}$), c_1 ($x=5 \text{ cm}$, $y=2.5 \text{ cm}$) and c_2 ($x=7.5 \text{ cm}$, $y=2.5 \text{ cm}$), shown in Figure 4(b) to have simulation. For MIT measurement, a sinusoidal current of 20 mA at 1 MHz flowed in the excitation coil and detection coil positioned on the model surface. For EIT measurement, an excitation current of 5 mA at 100 KHz flowed in the electrode of radius 2 cm and height 4 mm, which insert partly in the hemisphere.

3.2. Simulation data analysis

Reconstruction is performed using finite element grids, with horizontal sections including 10728 elements and 4787 nodes and vertical sections including 5461 elements and 2476 nodes.

Resolution is used to evaluate the concentration of the reconstructed image. When the value of the finite element exceeds half of the maximum imaging range, this point is defined as the half-amplitude value set. Resolution is defined as the root of the ratio of the half-amplitude value set to the sum of the imaging range. As from the definition, a smaller resolution represents clearer imaging identification of the reconstruction image. The resolution is calculated as a square root of the ratio between the area of the HA set (A_{HA}) and the domain area (A_0), as in the following equation:

$$\text{Res} = \sqrt{A_{HA} / A_0} \quad (1)$$

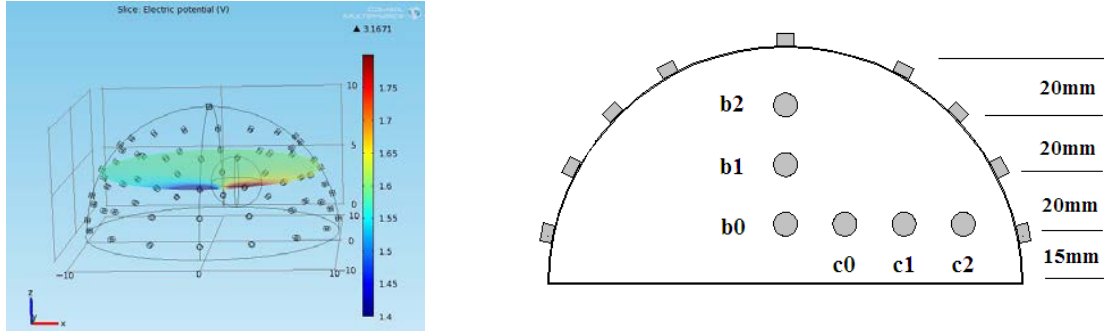


Fig. 4. (a) Diagram of the simulation model and (b) EIT Measurement Position Diagram.

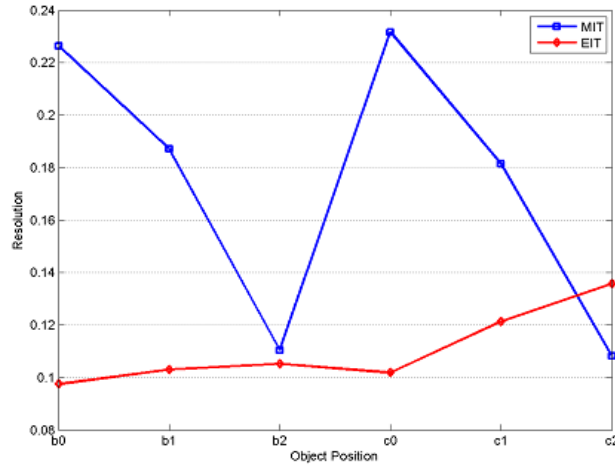


Fig. 5. Comparison of resolution simulation.

As in Figure 5, MIT has the lowest resolution when the measured object is near the center of the model. As the measured object moves toward the edge, the secondary magnetic field gets stronger, and the location of the object gets clearer. For EIT, we can see that the resolutions of the entire imaging area are much more stable, because of better current penetration. While the measured object approach the edge, the current field fluctuates due to boundary effects, which leads to imaging variations.

Position error can directly reflect the accuracy of the imaging result. The position of the measured object in the imaging area is defined as the following relationship:

$$Pos = \sum_m \sigma_m \cdot p_m / \sum_m \sigma_m \tag{2}$$

p_m is the position of the measured object in the finite element (x_m, y_m) , and σ_m is the conductivity of the measured object.

Relative position error is defined as the ratio of the position center of the reconstructed image to the position center of the foreign body. A smaller position error indicates that the foreign body position of the reconstructed image is close to the actual position center of the foreign body.

The characteristics of the two imaging methods can be seen from Figure 6. The detection coils are on the object surface for the MIT method, so the locating effect is better when the conductivity disturbance is located near the object surface, such as the position of b2 and c2. For the EIT method,

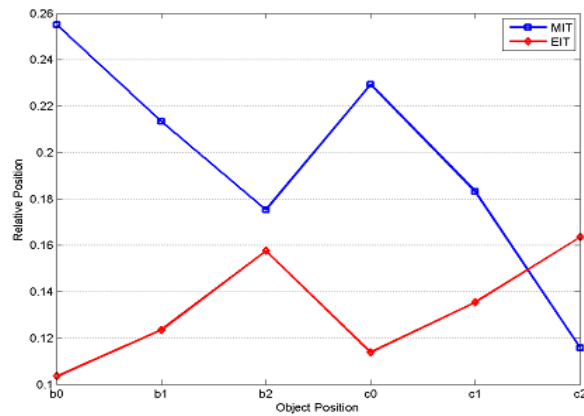


Fig. 6. Comparison of position error simulation.

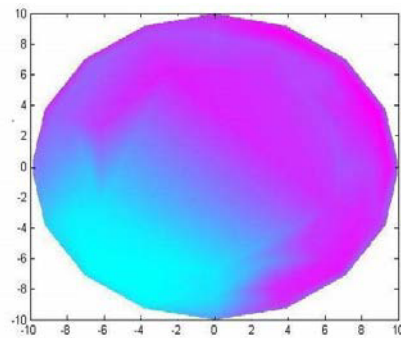
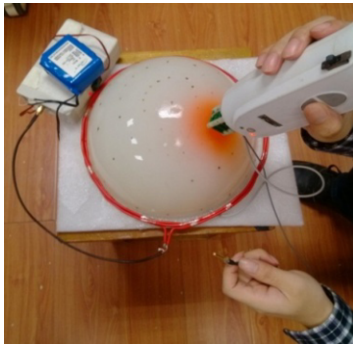


Fig. 7. (a) Schematic of Physics Experiments and (b) Plane Projection of MIT.

high current density corresponds to high system sensitivity in the middle of the current field, so the object position is located more accurately. As the distribution of current changes near the edge, the position error gets larger.

4. Physical experiment analysis

To obtain the actual image, we built a hemispherical agar model, which chooses agar with a conductivity of 0.1 S/m as the background material in Figure 7(a). In order to achieve accurate measurements, 65 basic measurement points mentioned above were marked on the model surface, and the 16 basic measurement points were used for the measurement of MIT. In the middle of the second layer and the third layer (see Figure 2(b)), a spherical agar block with a radius of 2.5 cm and a volume of 65 mm³ was placed to simulate anomalous human tissue, and the conductivity of this agar block was 0.6 S/m.

The imaging result of the plane projection of MIT is shown in Figure 7(b). This method provides roughly the position of the foreign body, but cannot accurately estimate the size and volume of foreign body, and also cannot recognize it in space. After EIT measurements were applied, it offers more useful information. The extracted results of different conductivity from the surface are shown in Figure 8, and these results consist of the measured results of the horizontal section and the measured

results of the vertical section.

The reconstructed images of the sections located in $x=-3, -4, -5$ and $z=3, 4, 5$ are shown in Figure 8. In the reconstructed images, the foreign body is not a regular sphere. The images located on the x section seem to have a trend toward two sides. The size of the foreign body in the images located on the z section is smaller than the actual foreign body. The reconstructed results of the foreign body in different sections are all close to the surface of the hemisphere, but there is poor sensitivity near the center of hemisphere. So in actuality, the algorithm should be analyzed and improved according to the characteristics of the measured object.

Figure 9 shows the three-dimensional and reconstructed images after the interpolation algorithm dealt with the multi-group data of sections. Different colors are used to distinguish the curved surface of different conductivities. The conductivity from one curved surface relates to the difference between background and foreign body and the system error, so it should be a number in 0.5~0.6. From the images, we can conclude that the achieved information is limited, and the reconstructed images feature few anomalies [12]. However, compared with the MIT method, the EIT method improves the reconstructed results, locates the foreign body more accurately, reconstructs the three-dimensional images and can provide much useful information, such as the depth and volume of the foreign body. It

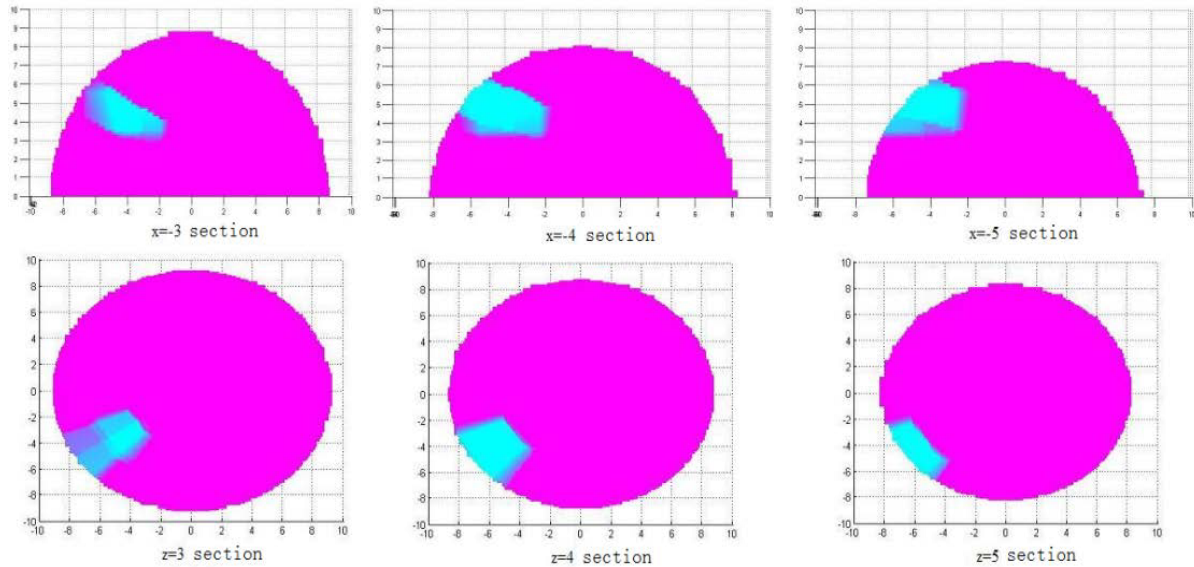


Fig. 8. Sectional results of electrical impedance imaging.

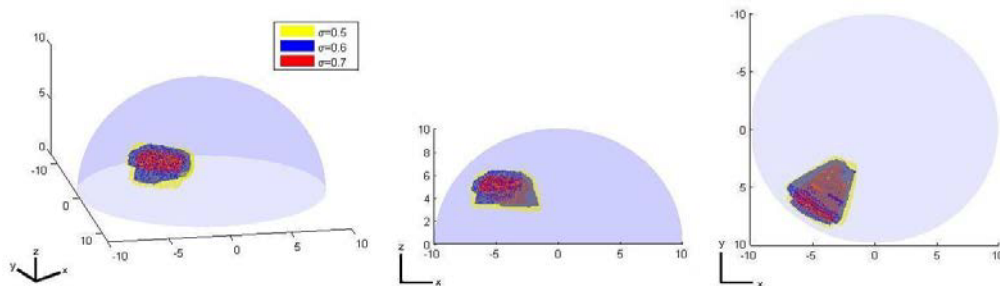


Fig. 9. The results of 3D reconstruction of the electrical impedance imaging system.

produces improved reconstructed results with better positions. Through the suitable conductivity from one curved surface, the size of the foreign body can generally be estimated.

5. Conclusion

In this paper, the composite system and measurement strategy were introduced. From the above experiments, we could conclude that EIT and MIT complement each other in measurement. On one hand, the MIT method achieves rapid measurement and accurately locates foreign bodies in measurement. On the other hand, the EIT method gets more useful information and improves the effect of reconstructed images. This system showed efficiency and high accuracy, which complements both the detections of edge and deep sections, greatly satisfies the clinical requirements.

Acknowledgment

The authors would like to thank the Program for Innovation Team Building at Institutions of Higher Education in Chongqing (The Innovation Team of Smart Medical System and Key Technology). This work was supported in part by the Chongqing Science and Technology Commission Young Talent Project (CSTC2013kjrc-qnrc10007) and the Chongqing Education Commission Research Project (KJ1400439).

References

- [1] D. Holder, *Electrical impedance tomography: methods, history and applications*, Institute of Physics, London, 2004, pp. 295-347.
- [2] H. Scharfetter, Roberto Casanas and Javier Rosell, Biological tissue characterization by magnetic induction spectroscopy: Requirements and limitations, *IEEE Transactions on Biomedical Engineering* **50** (2003), 870-880.
- [3] Mingxin Qin, Yun Wang, Xiaoyan Hu, et al., Study of MIT phase sensitivity for detecting a brain edema based on FDTD method, 1st International Conference on Bioinformatics and Biomedical Engineering, Wuhan, China, 2007, 660-663.
- [4] David S. Holder and H. Griffiths, *Electrical impedance tomography: Methods, history and applications*, in: *Magnetic Induction Tomography*, Chapter 8, IOP Publishing, London, 2005, pp. 213-238.
- [5] TCI (Technology Commercialization International Inc.) Centillion, *Advanced Digital Imaging System for Breast Cancer Detection*, 2003.
- [6] I. Frerichs, J. Hinz, P. Herrmann, G. Weisser, G. Hahn, M. Quintel and G. Hellige, Regional lung perfusion as determined by electrical impedance tomography in comparison with electron beam CT imaging, *IEEE Transactions on Medical Imaging* **21** (2002), 646-652.
- [7] International Commission on Non-Ionizing Radiation Protection, Guidelines for limiting exposure to time-varying electric, magnetic and electromagnetic fields (up to 300 GHz), *Health Physics* **97** (1998), pp. 257-258.
- [8] N.G. Gencer and M. Nejat Tek, Electrical conductivity imaging via contactless measurements, *IEEE Transaction on Medical Imaging* **18** (1999), 617-627.
- [9] C.H. Riedel, M. Keppelen, S. Nani and O. Dossel, Planar system for magnetic induction conductivity measurement using a sensor matrix, *Physiological Measurement* **25** (2004), 403-411.
- [10] Wei He, Peng Ran, Zheng Xu, et al, 3D electrical impedance tomography represented by reconstructed planes in a semispherical electrode array model, *International Journal of Applied Electromagnetics and Mechanics* **41** (2013), 433-446.
- [11] H. Griffiths, W.R. Stewart and W. Gough, Magnetic induction tomography: A measuring system for biological tissues, *Annals of the New York Academy of Sciences* **873** (1999), 335-345.
- [12] Wei He, Peng Ran, Zheng Xu, et al., A 3D visualization method for bladder filling examination based on EIT, *Computational and Mathematical Methods in Medicine* **2012** (2012), 528096.